

Aluminum as a source of background in low background experiments

B. Majorovits^{a,1}, I. Abt^a, M. Laubenstein^b, O. Volynets^a

^a *MPI für Physik, Föhringer Ring 6, 80805 Munich, Germany*

^b *Laboratori Nazionali del Gran Sasso, INFN, S.S.17/bis, km 18+910, I-67100 Assergi (AQ), Italy*

Abstract

Neutrinoless double beta decay would be a key to understanding the nature of neutrino masses. The next generation of High Purity Germanium experiments will have to be operated with a background rate of better than 10^{-5} counts/(kg y keV) in the region of interest around the Q value of the decay. Therefore, so far irrelevant sources of background have to be considered. The metalization of the surface of germanium detectors is in general done with aluminum. The background from the decays of ^{22}Na , ^{26}Al , ^{226}Ra and ^{228}Th introduced by this metalization is discussed. It is shown that only a special selection of aluminum can keep these background contributions acceptable.

¹ corresponding author. Tel.: +49 89 32354 262, FAX: +49 89 32354 528. Address: MPI für Physik, Föhringer Ring 6, 80805 München, E-mail: bela@mppmu.mpg.de

1 Introduction

High Purity Germanium (HPGe) detectors are extremely sensitive spectrometers, used to search for rare events, such as neutrinoless double beta decays or dark matter scattering off nuclei [1, 2, 3]. In order to rule out the possibility of an inverted neutrino mass hierarchy, a neutrino with a Majorana mass as low as 10 meV has to be excluded. The low event rates expected, require very low background environments and a very high target mass.

An HPGe based neutrinoless double beta decay experiment would need an active mass of ≈ 1 ton and a background level below 10^{-5} counts/(kg y keV) around the Q-value of the double beta decay of ^{76}Ge at 2039 keV. This requires a reduction of the background rate by three to four orders of magnitude with respect to the current state of the art. This necessitates the investigation of so far unimportant background contributions. Here, the effects of ^{26}Al and ^{22}Na , cosmogenically produced in aluminum, are investigated.

As it is not trivial to obtain radio-pure aluminum [4], it is usually avoided close to the active elements of low background experiments. However, aluminum is commonly used to metallize HPGe detector surfaces. For low background applications, great care is often taken to use especially selected "Ultra Low Background" (ULB) aluminum [5, 6]. However, even if U- and Th- free aluminum is used, ^{26}Al , cosmogenically produced, is not removed during the refinement process.

The isotope ^{26}Al has a Q-value of 4.0 MeV and a half life of $7.17 \cdot 10^5$ years [7]. In 81.7 %, it decays by emission of a positron, an electron and a 1808.7 keV gamma to ^{26}Mg . Thus, it can deposit around ≈ 2 MeV inside the detector.

The isotope ^{22}Na can also be cosmogenically produced in aluminum. It has a Q-value of 2.84 MeV and a half life of 2.6 years [7]. In 90.3 %, it decays by emission of a positron and a 1274.5 keV gamma to ^{22}Ne . During the refining process leading to commercially available aluminum, it is efficiently separated. However, as the half life is relatively short, equilibrium between production and decay rate is regenerated within the relatively short time span of a few years.

2 Cosmogenic production of ^{26}Al and ^{22}Na from ^{27}Al

Aluminum consists ≈ 100 % of the isotope ^{27}Al . Small quantities of the ground state of ^{26}Al , $^{26}\text{Al-g}$, can be produced cosmogenically through the reactions $^{27}\text{Al}(n,2n)^{26}\text{Al-g}$ and $^{27}\text{Al}(p,np)^{26}\text{Al-g}$. The isotope ^{22}Na can be produced by the reactions $^{27}\text{Al}(n,2p4n)^{22}\text{Na}$ and $^{27}\text{Al}(p,3p3n)^{22}\text{Na}$.

If the energy dependent production cross-sections, $\sigma(E)$, for the reactions under consideration and the differential neutron and proton fluxes as a function of energy, $\frac{\partial \Phi_{n/p}}{\partial E}$, are known, the total production rates can be calculated as

$$dN/dt = N_0 \int_0^\infty \frac{\partial \Phi_{n/p}}{\partial E} \cdot \sigma(E) dE, \quad (1)$$

where N_0 is the number of target nuclei. In equilibrium, the decay and production rates of the considered isotope are equal.

Additionally, production of ^{26}Al and ^{22}Na through negative muon capture and spallation reactions induced by fast through-going muons is possible.

2.1 Production cross-sections

The measured production cross-sections of the $^{27}\text{Al}(n,2n)^{26}\text{Al}$ -g reaction above the production threshold of 13.55 MeV up to neutron energies of 60 MeV are summarized in Fig. 1. Above 15 MeV, three measurements exist [8, 9, 10]. The cross-section peaks at 20 MeV according to Nakamura et al. [8] and Pavlik et al. [9]. In Wallner et al. [10] the highest available neutron energy was 19 MeV. The measured cross-sections of the latter reference are consistent with the data shown in Nakamura et al. They are roughly a factor of two higher than the cross-sections shown in Pavlik et al. For the calculation of the number of cosmogenically produced ^{26}Al nuclei by neutrons, a polynomial fit to the cross-sections from Wallner et al. and Nakamura et al. is used up to 20 MeV and values recommended by Euratom/UKAEA [11] were used for energies between 20 MeV and 60 MeV. The recommended excitation function is also shown in Fig. 1. Up to 20 MeV, the recommendation coincides with the polynomial fit to the Wallner et al. and Nakamura et al. data. Above 60 MeV, a constant cross-section of 20 mb was assumed.

Measured cross-sections [12, 13, 14, 15, 16] for the reaction $^{27}\text{Al}(p,pn)^{26}\text{Al}$ -g, including a polynomial fit, are shown in Fig. 2. The fit was used for the calculation of the production rate through this excitation channel.

There are little data on ^{22}Na production cross-sections from the reaction $^{27}\text{Al}(n,2p4n)^{22}\text{Na}$. An integrated cross-section of about 8 mb [17] has been measured from the threshold of 23 MeV up to 750 MeV. Cross-sections of (15.2 ± 5.5) mb and (8.2 ± 1.9) mb at energies of 110.8 MeV and 112 MeV, respectively, have also been reported [18]. These values agree within the uncertainties. They are displayed in Fig. 3. The available data for the reaction $^{27}\text{Al}(p,3p3n)^{22}\text{Na}$ [19, 20, 21, 22] are also presented in Fig. 3.

As no energy dependent measurements of the cross-section for the reaction $^{27}\text{Al}(n,2p4n)^{22}\text{Na}$ were available, it was assumed that the cross-sections for neutrons and protons as a function of energy are the same. For energies above the Coulomb barrier of a reaction, this assumption is justified due to isospin symmetry. The Coulomb barrier is around a few MeV for the reactions under investigation. For the calculations of the production rates from the reaction $^{27}\text{Al}(n,2p4n)^{22}\text{Na}$ and $^{27}\text{Al}(p,3p3n)^{22}\text{Na}$, a polynomial fit to the proton excitation function data, displayed in Fig. 3, was used.

83 2.2 Secondary neutron and proton fluxes at sea level

84 Two sets of neutron flux measurements [23, 24] at sea level around New York are shown
85 in Fig. 4. The measurements agree within an order of magnitude. However, for energies
86 below 100 MeV and above 1000 MeV, they still differ significantly.

87 The secondary proton flux at sea level is significantly lower than the neutron flux at
88 energies relevant for the production of ^{26}Al and ^{22}Na . A polynomial fit to the proton
89 spectrum measured in Karlsruhe, Germany [25] is shown in Fig. 5.

90 For the calculation of the expected production rates, the more conservative neutron spec-
91 trum from [23] and the fit to the proton spectrum were used, unless otherwise stated.

92 2.3 Exposure of bauxite to secondary cosmic rays

93 Aluminum is refined from bauxite deposits that were predominantly formed by weathering
94 [26] during several periods in Earth history. The currently mined deposits consist mainly
95 of lateral sheets that have rested on or close to the surface for the past million years. The
96 top-soil overburden above the bauxite layer is often negligible [27] or has a thickness of
97 less than a meter for major mining sites [28]. The bauxite layers themselves are usually
98 as thin as 2 m to 4 m [28]. Underground mines, exploiting pockets of bauxite, are mainly
99 located in Southern Europe and Hungary and have a small market share.

100 The top soil above the bauxite layers of mining sites and the self shielding of the 2 –
101 4 m thick bauxite layers reduce the secondary cosmic ray flux and thus the cosmogenic
102 activation of the aluminum yielding ^{26}Al and ^{22}Na . In order to account for the shielding
103 by the top soil and the self shielding of the bauxite layer, a Monte Carlo simulation was
104 performed. The MaGe [29] framework based on GEANT4 [30] was used.

105 Two scenarios, typical for major bauxite mining sites, were taken into account: a top soil
106 free mining site (like WEIPA, Australia [27]) and a site with 1 m quartz sand overburden.
107 The composition of the simulated bauxite was chosen according to the one reported for
108 the WEIPA site [27].

109 For both scenarios, top soil free and 1 m top soil, the neutron and proton fluxes were
110 simulated at different depths in the bauxite layer: for depths between 0 m and 0.5 m
111 in steps of 0.1 m and for depths between 0.5 m and 2.0 m in steps of 0.5 m. The fluxes
112 calculated for the different depths were averaged to obtain the mean neutron spectra for
113 a bauxite layer with 2 m thickness with and without top soil.

114 The spectra for neutrons and protons are shown in Fig. 4 and Fig. 5, respectively. The
115 averaged spectra were used for calculating realistic ^{26}Al and ^{22}Na production rates within
116 a 2 m bauxite layer.

117 2.4 Calculated ^{26}Al and ^{22}Na production rates

118 The calculated differential production rates of ^{26}Al and ^{22}Na for the previously described
119 neutron and proton spectra at sea level and for different shielding scenarios are shown in
120 Fig. 6 and Fig. 7, respectively. The production rate is significantly lower for the spectrum
121 of [24] than for the selected standard [23] below 100 MeV.

122 Self shielding by a 2 m bauxite layer does reduce the differential production rates of ^{26}Al
123 and ^{22}Na by a factor of roughly 4–10 with respect to the sea level production rate,
124 depending on the neutron and proton energy.

125 The integrated production rates of ^{26}Al and ^{22}Na are given in Table 1. The reference
126 neutron flux [23] at sea level without overburden results in a production rate of 142 (56)
127 ^{26}Al (^{22}Na) nuclei per year and gram aluminum. The reduced neutron flux [24] at sea level
128 results in a production rate of roughly 80 (43) ^{26}Al (^{22}Na) nuclei per gram aluminum per
129 year. The higher production threshold of ^{22}Na reduces this difference in the production
130 rate of ^{22}Na compared to the one of ^{26}Al .

131 The mean ^{26}Al (^{22}Na) production rate due to the [23] in a 2 m thick bauxite layer is 21
132 (11) ^{26}Al (^{22}Na) nuclei per year and gram aluminum.

133 If another 1 m of quartz sand overburden is assumed, the production rate through sec-
134 ondary neutrons drastically drops to 1.4 (1.0) ^{26}Al (^{22}Na) nuclei per year and gram of
135 aluminum.

136 The expected production rate at sea level without overburden from protons is 17 (3) ^{26}Al
137 (^{22}Na) nuclei per gram aluminum per year. It becomes negligible if self shielding or an
138 additional layer of top soil are taken into account.

139 In total in equilibrium in a 2 m bauxite layer without top soil 23 ^{26}Al decays per gram
140 aluminum per year are expected. At sea in equilibrium 65 ^{22}Na decays are expected per
141 gram aluminum per year.

142 Muon capture and spallation reactions induced by through-going muons can also lead
143 to the production of ^{26}Al and ^{22}Na in quartz. The contribution due to this production
144 channel at sea level is roughly 4% [31]. As neutrons and protons are absorbed more
145 efficiently in matter than muons, the fraction of ^{26}Al and ^{22}Na produced by negative
146 muon capture and fast muons increases with increasing overburden.

147 To estimate the realistic contribution of the production rate due to muons, the production
148 rates deeper inside the bauxite layer have to be considered. This was done for the case
149 of no top soil and a 2 m thick bauxite layer. The density of bauxite is very sensitive
150 to the grain size [32]. It ranges between 1.3 g/cm³ for fine grain up to 3.5 g/cm³ for
151 dense bauxite with a large quartz content. Thus, a 2 m bauxite layer will correspond to
152 2.6–7 meter water equivalent, mwe, depending on the mining site. At 2.6 mwe (7 mwe)
153 the contribution of muons to the ^{26}Al production in quartz is 10% (75%) [31]. For deep
154 bauxite layers with non negligible top soil, the production channel through muons will

155 be dominating. For the case of shallow, low density bauxite mines, considered here, the
 156 production rate through muons is small. As there are already large uncertainties in the
 157 secondary neutron and proton fluxes, the muon contribution is neglected from now on.

158 **3 Comparison to measurements of cosmogenically pro-** 159 **duced ^{26}Al in quartz**

160 The isotope ^{26}Al is a well known tracer for erosion rates in geology [31]. The production
 161 rates of ^{26}Al have mainly been measured in quartz samples. In glacially exposed surface
 162 layers, an average production rate of 374 ± 28 ^{26}Al nuclei per g quartz per year has been
 163 measured at an elevation of 3340 m [33]. This can be translated into a production rate at
 164 sea level of 36.8 ± 2.7 (stat.) ^{26}Al nuclei per g quartz per year. This is in good agreement
 165 with recent measurements from [34]. These measurements can be used to validate the
 166 calculation method used for production rates in Bauxite.

167 The excitation functions for ^{26}Al in ^{28}Si for neutrons are only available for energies be-
 168 tween 25 MeV and 36 MeV [35]. At higher energies, only proton excitation functions are
 169 available [12, 36]. As the measured neutron [35] and proton [14] cross-sections are in very
 170 good agreement at energies between 25 MeV and 35 MeV, it can be assumed that the
 171 neutron excitation function is about equal to the measured proton excitation function at
 172 all energies. At high energies, excitation functions for neutrons and protons are in general
 173 expected to be the same due to isospin symmetry.

174 Using a polynomial fit to the excitation function [35] and the unshielded neutron (proton)
 175 spectrum at sea level from [23] ([25]), a ^{26}Al production rate in quartz at sea level of 44 (6)
 176 nuclei per gram quartz is expected. Considering the large uncertainties in the secondary
 177 cosmic ray flux variations with geographic location and the uncertainties in the exposure
 178 histories of the measured samples, this is in good agreement with the experimental values.

179 The good agreement between calculation and measurement shows that the method to
 180 estimate the activities of ^{26}Al and ^{22}Na in bauxite samples can be trusted to roughly a
 181 factor of two.

182 **4 Background expectations due to ^{26}Al and ^{22}Na**

183 The contamination of any sample of aluminum depends on its history. Equilibrium be-
 184 tween production rate and decay of an isotope will be reached after a few half lives. This
 185 is the case after a few million (ten) years for ^{26}Al (^{22}Na). For the case of a 2 m bauxite
 186 layer without top soil, in equilibrium a ^{26}Al activity of 23 decays per year is expected per
 187 gram aluminum, see Table 1.

188 The contamination with ^{26}Al is not affected by the refining process. The expected equi-
 189 librium activity for a 2 m bauxite deposit without top soil is 0.8 mBq/kg. For ease of
 190 scaling, an activity of 1.0 mBq/kg was used for the background estimates. Due to its long
 191 half life, the background from ^{26}Al is constant during any experiment.

192 The contamination with ^{22}Na is eliminated effectively during the refining process. Thus
 193 for ^{22}Na it is the exposure history after aluminum refinement that determines its activity.
 194 After one half life (2.6 years) of exposure to cosmic rays, the decay rate is equal to half
 195 of the production rate. For no overburden at sea level, this corresponds to 1.0 mBq/kg.
 196 This value was assumed to estimate backgrounds. For underground experiments, the ^{22}Na
 197 activity decreases significantly after a few years.

198 Significant ^{228}Th contaminations of the order of mBq/kg have been measured in ULB
 199 aluminum. For the background estimate, 1.0 mBq/kg ^{228}Th and ^{226}Ra activities were
 200 assumed.

201 Typically, the thickness of the metalization on HPGe detectors is around 300 nm. Thus
 202 for a typical detector with 7.0 cm height and 7.5 cm diameter, roughly

$$7 \text{ cm} \cdot \pi \cdot 7.5 \text{ cm} \cdot 300 \text{ nm} \cdot 2.7 \frac{\text{g}}{\text{cm}^3} = 13.4 \text{ mg} \quad (2)$$

203 of aluminum are deposited on the detector surface. Taking the production rates expected
 204 from the neutron flux from [23], roughly $159 \text{ decays/g} \cdot 0.0134 \text{ g} \approx 2.1$ ^{26}Al decays per
 205 detector per year and $28 \text{ decays/g} \cdot 0.0134 \text{ g} \approx 0.4$ ^{22}Na decays per detector per year are
 206 expected.

207 A Monte Carlo simulation of $25.2 \cdot 10^6$ ^{22}Na , ^{26}Al and ^{228}Th decays each, was performed.
 208 The MaGe [29] framework based on GEANT4 [30] was used to simulate an array of true
 209 coaxial HPGe detectors corresponding to a nominal phase II arrangement of GERDA [1].
 210 The array consisted of seven strings with three detectors each, with the strings being
 211 aligned at the same height. The configuration had hexagonal closest packing with a
 212 closest radial distance of 15 mm between the detector surfaces. The distance in height
 213 between the detector boundaries was 60 mm. All detectors were true coaxial n-type 18-
 214 fold segmented with 75 mm diameter and 70 mm height and a bore hole diameter of 10 mm
 215 [37]. The ^{22}Na , ^{26}Al , ^{226}Ra and ^{228}Th contaminations were simulated as being randomly
 216 distributed on the metalized surfaces of all detectors.

217 The results of the simulation are listed in Table 2. Background events induced by photon
 218 interactions can be identified through the event topologies by requiring the energy to
 219 be deposited in a single detector or in case of segmented detectors a single segment [38].
 220 Applying single segment cuts compared to single detector cuts can reduce the background
 221 in the region of interest by typically an order of magnitude, depending on the background
 222 source. The simulated spectra, normalized to the expected number of decays per year and
 223 kilogram of germanium, without any cut, with single detector cut and with single segment
 224 cut are shown in Figs. 8, 9, 10 and 11. The last row of Table 2 gives the tolerable activity
 225 of the considered nuclide to restrict the background to $10^{-6} \text{ counts}/(\text{kg y keV})$ with single
 226 segment cut applied. While for ^{22}Na an activity of a few mBq/kg can be tolerated, the

227 restrictions on ^{26}Al , ^{226}Ra and ^{228}Th contaminations are more severe at the hundreds of
 228 $\mu\text{Bq/kg}$ level.

229 The resulting spectra in the energy window between 1940 keV and 2140 keV are shown in
 230 the insets of Figs. 8, 9, 10 and 11. For ^{26}Al , the background rate in the region of interest
 231 is approximately constant. A background rate of up to $0.17 \cdot 10^{-5}$ counts/(kg y keV) is
 232 expected for a single segment cut. The background expected from ^{22}Na is $\approx 2.6 \cdot 10^{-7}$
 233 counts/(kg y keV) and thus less critical. The contribution due to a 1.0 mBq/kg ^{228}Th
 234 contamination is expected to be $0.5 \cdot 10^{-5}$ counts/(kg y keV), while for ^{226}Ra it is $0.26 \cdot 10^{-5}$
 235 counts/(kg y keV).

236 If no cut based on event topologies is made, the background rate is higher by roughly one
 237 order of magnitude. In this case the background will be at levels of up to 10^{-4} counts/(kg y keV).
 238 A single detector cut reduces the backgrounds due to the decays of ^{22}Na and ^{26}Al by fac-
 239 tors of 1.4 and 3.2, respectively. A single segment gives suppression factors of 10 and 30
 240 for ^{22}Na and ^{26}Al , respectively. For ^{226}Ra and ^{228}Th , the single segment cut gives only
 241 suppression factors of 2.6 and 4.5, respectively.

242 5 Measurements of ^{26}Al , ^{22}Na and primordial nuclides 243 in high purity aluminum samples

244 Measurements of five different ULB aluminum samples were performed. All measurements
 245 were done to qualify low background aluminum for its use in low background detectors.
 246 The measurements of the samples were carried out at the Laboratori Nazionali del Gran
 247 Sasso (LNGS) using the GEMPI [39] and GeCRIS [40] detectors. Details of the samples
 248 and measured activities or limits are listed in Table 3. Some of these results were published
 249 earlier [5, 6]. Three of the five samples show a non zero ^{26}Al activity. The activities lie
 250 in the range of 0.2–0.6 mBq/kg. This translates into 6.3–18.9 ^{26}Al decays per year per
 251 gram aluminum.

252 The highest measured activity of 0.6 mBq/kg of the Kryal #1 sample, see Table 3, is close
 253 to the one calculated for a 2 m bauxite layer without top soil. However, for the Kryal
 254 #2 sample, an upper limit of <0.26 mBq/kg was established. It is remarkable that the
 255 ^{26}Al activities of the five samples differ so significantly. This indicates that the bauxite
 256 used for the production of the ULB aluminum was mined at sites with different top soil
 257 overburden or with different bauxite layer thicknesses or histories. It also shows that some
 258 of the commercially available bauxite must have originated from mines with no top soil
 259 overburden and shallow bauxite layers.

260 One of the samples shows a ^{22}Na activity of 0.7 ± 0.3 mBq/kg corresponding to 22 ± 9 ^{22}Na
 261 decays per gram aluminum per year. This is in very good agreement with the assumption
 262 of exposure of the ULB aluminum to sea level secondary cosmic rays for about two years
 263 before the screening measurement. Alternatively the sample could have been exposed to

264 increased cosmic radiation by air transport.

265 In some of the ULB aluminum samples, also ^{226}Ra or ^{228}Th activities were measured. In
266 all cases the ^{228}Ra activity was considerably lower than the ^{228}Th activity, suggesting that
267 the ^{232}Th chain was not in secular equilibrium. It is not clear, whether ^{228}Th (and possibly
268 ^{232}Th) stems from initial contaminations of the bauxite or from impurities introduced to
269 the ULB aluminum during the refining process.

270 6 Conclusion

271 The detailed geological history of a given mining site determines the exposure of the baux-
272 ite to neutrons and protons. Therefore, the source of the aluminum has to be controlled
273 and the aluminum used has to be screened for radio-impurities with sufficient sensitivity.

274 The contamination with ^{26}Al can be avoided by using aluminum refined from underground
275 bauxite deposits. The contamination with ^{22}Na has to be avoided by restricting the time
276 of the aluminum stored above ground. The calculations show that the background induced
277 by ^{26}Al , ^{226}Ra , ^{228}Th and to a lesser extent ^{22}Na in the metalization can be significant, if
278 proper care is not taken.

279 ^{26}Al has been measured in some ULB aluminum samples with activities consistent with
280 the prediction of the calculations taking into account a 2 m thick bauxite layer without
281 or with very little top soil. In one of the ULB aluminum samples ^{22}Na was found with an
282 activity consistent with two years of sea level exposure to cosmic rays.

283 The simulations show that for neutrinoless double beta decay experiments using HPGe
284 detectors with metalization, the material used to metallize the surfaces has to be care-
285 fully screened for radio-impurities. For the case of n-type HPGe detectors with a diam-
286 eter of 7.5 cm and a height of 7.0 cm, maximal radio-impurities of less than 0.6 mBq/kg,
287 3.3 mBq/kg, 0.2 mBq/kg and 0.2 mBq/kg are required in order not to exceed individual
288 background contributions of larger than 10^{-6} counts/(kg y keV) from ^{22}Na , ^{26}Al , ^{226}Ra
289 and ^{228}Th , respectively. ULB HPGe detectors with the sensitivity required to test ULB
290 aluminum with this sensitivity are available [39, 40].

291 In order to avoid dangerous radio-impurities, the aluminum for the next generation neu-
292 trinoless double beta-decay experiments has to be produced from bauxite from mines with
293 sufficient top soil overburden. Otherwise, the cosmogenically produced isotope ^{26}Al will
294 create a background level limiting the sensitivity of the experiment.

295 **7 Acknowledgment**

296 We would like to thank G. Heusser for the careful reading of the manuscript, many
297 valuable comments and the information about the availability of the HPGe screening
298 measurements of ULB aluminum.

299 **References**

- 300 [1] I. Abt et al., arXiv:hep-ex/0404039 and S. Schönert et al., Nucl. Phys. Proc. Suppl.
301 **145**(2005)242
- 302 [2] The CDMS collaboration, Science **327**(2010)1619
- 303 [3] E. Armengaud et al., Phys. Lett. B **687**(2010)294, arXiv:0912.0805
- 304 [4] G. Heusser, Ann. Rev. Nucl. Part. Sci., **45**(1996)543
- 305 [5] P. Loaiza et al., NIM A **634**(2011)64
- 306 [6] M. Köhler et al, J. Appl. Rad. Isot. **67**(2009)736
- 307 [7] M.M. Bé et al., LNHB website, http://www.nucleide.org/DDEP_WG/DDEPdata_by_A.htm
- 308 [8] T. Nakamura et al., Phys. Rev. C **43**(1991)1831
- 309 [9] A. Pavlik et al., Phys. Rev. C **57**(1998)2416
- 310 [10] A. Wallner, Eur. Phys. J. A **17**(2003)285
- 311 [11] R.A. Forrest, J. Kopecky, UKAEA FUS 529, Euratom/UKAEA Fusion, May 2006
- 312 [12] T. Schiek et al., NIM B **114**(1996)91
- 313 [13] B. Dittrich, NIM B **52**(1990)588
- 314 [14] M. Furukawa et al., Nucl. Phys. A **174**(1971)539
- 315 [15] R. Michel et al., NIM B **129**(1997)153
- 316 [16] S. Shibata, J. Phys. C. **48**(1993)2617
- 317 [17] J. Sisterson, J. Ullmann, NIM B **234**(2005)419
- 318 [18] J. Sisterson, NIM B **261**(2007)993
- 319 [19] E. Buthelezi et al., Appl. Rad. Isot. **64**(2006)916
- 320 [20] Y. Titarenko et al., INDC report **434**(2003)88

- 321 [21] G.L. Morgan, NIM B **211**(2003)297
- 322 [22] G.F. Steyn, Appl. Rad. Isot. **42**(1990)315
- 323 [23] J.F. Ziegler, IBM Res. Develop. **42**(1998)117, J.F. Ziegler, IBM Res. Develop.
324 **40**(1996)19
- 325 [24] M.S. Gordon et al., IEEE Trans. Nucl. Sci. **51**(2004)3427
- 326 [25] H. Filthuth, Suppl. Nuovo Cimento, Vol. IV, Serie X N.2 (1956)906
- 327 [26] I. Valetton, Catena **21**(1994)99
- 328 [27] G. Taylor et al., Austral. J. Earth Sci., **55** Suppl. 1(2008)S45
- 329 [28] R. Quinkertz, PhD, RWTH Aachen, Germany, 2002, <http://d-nb.info/965686876>
- 330 [29] M. Boswell et al., arXiv:1011.3827
- 331 [30] S. Agostinelli et al., NIM A **506**(2003)250
- 332 [31] B. Heisinger et al., NIM B **123**(1997)341
- 333 [32] Y. Pivinskii, Refrac. Ind. Ceram. **44**(2003)399
- 334 [33] K. Nishiizumi et al., J. Geophys. Res. **17**(1989)17907
- 335 [34] M.M. Goethals, Earth and Planetary Sci Lett. **284**(2009)187
- 336 [35] M. Imamura et al., NIM B **52**(1990)595
- 337 [36] M. Michel et al. NIM B **103**(1995)183
- 338 [37] I. Abt et al., NIM A **577**(2007)574
- 339 [38] I. Abt. et al., NIM A **570**(2007)479
- 340 [39] G. Heusser, M. Laubenstein, H. Nider in Radionuclides in the Environment, edited
341 by P. P. Povinec and J. A. Sanchez-Cabeza, Else vier, Amsterdam, pp. 495-510, 2006
- 342 [40] P. Belli et al., Phys. REV. C **83**(2011)034603

	²⁶ Al		²² Na	
	[(g y) ⁻¹]	[mBq/kg]	[(g y) ⁻¹]	[mBq/kg]
Neutrons at sea level	142	4.5	56	1.8
Neutrons [24]	80	2.5	43	1.3
Neutrons in 2 m bauxite	21	0.67	11	0.4
Neutrons, 1 m quarz sand + 2 m bauxite	1.4	0.04	1.0	0.03
Protons at sea level	17	0.54	8.7	0.10
Protons in 2 m bauxite	2.1	0.07	1.0	0.03
Protons, 1 m quarz sand + 2 m bauxite	0.1	0.0	0.01	0.0
n+p, 2m bauxite	23	0.74		
sea level, half equilibrium			32	1.0

Table 1: Calculated production rates and corresponding activities for secular equilibrium for ²⁶Al and ²²Na for different overburden scenarios: at sea level without any overburden, for a 2 m thick bauxite layer accounting for self absorption and for a 2 m thick bauxite layer underneath 1 m top soil. Secondary neutron spectra from [23] were assumed if not otherwise stated. The last two lines give a realistic prediction for ²⁶Al, where equilibrium is assumed after millions of years in a 2 m bauxite layer, and for ²²Na, where half equilibrium is reached at the surface after refinement of the aluminum.

Nuclide	Number of events in RoI			Background index			Allowed activity [mBq/kg]
	total	SD cut	SS cut	total	SD cut	SS cut	
				[10 ⁻⁵ Counts/(kg y keV)]			
²² Na	209 374	122 942	5 335	0.26	0.16	0.03	3.3
²⁶ Al	843 308	26 828	30 670	4.62	1.45	0.17	0.6
²²⁸ Th	419 903	149 115	93 647	2.19	0.78	0.49	0.2
²²⁶ Ra	127 017	93 907	49 846	0.67	0.49	0.26	0.4

Table 2: The first three columns show the simulated number of events which have an integrated energy deposit between 1940 keV and 2140 keV in the detector array (total), in a single detector (SD cut) and in a single segment (SS cut) of a detector. The resulting background indices expected for an activity of 1.0 mBq/kg in this energy window are given in the next three columns. The last column lists the activity allowed to restrict the background to 10⁻⁶ counts/(kg y keV).

Sample	²⁶ Al	²² Na	²²⁶ Ra	²²⁸ Ra	²²⁸ Th	⁴⁰ K
Kryal, Hydro Al., UTH 1	0.6±0.3	0.7±0.3	< 0.38	<1.9	<1.7	<21
Kryal, VAW, UTH 0.25	< 0.26	< 0.15	<0.58	<1.2	<0.65	<22
Highpural, VAW	< 0.45	< 0.37	<3.7	12±2	47±5	<5.5
ULB I [6]	0.2±0.1	< 0.32	<0.7	<0.9	3.8±0.7	4.9 ±1.8
ULB II [5]	0.38^{+0.19}_{-0.14}	< 0.18	0.27±0.19	< 0.11	1.4±0.2	1.1^{+0.2}_{-0.1}

Table 3: Measured ²⁶Al, ²²Na, ²²⁶Ra, ²²⁸Th and ⁴⁰K activities of ULB aluminum samples in mBq/kg.

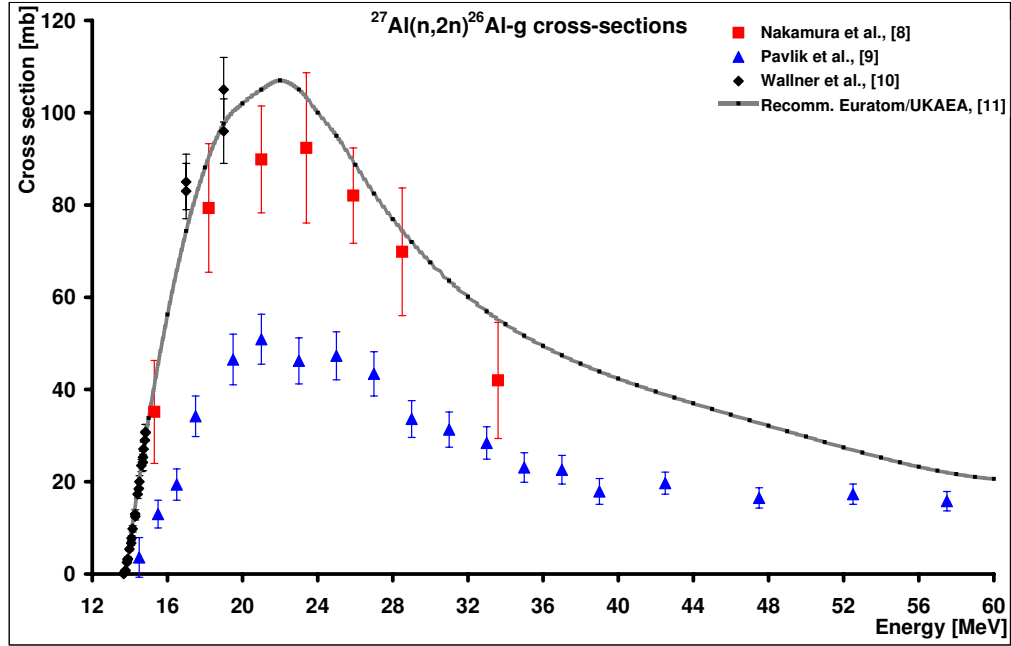


Figure 1: Measured production cross-sections for the reaction $^{27}\text{Al}(n,2n)^{26}\text{Al-g}$ [8, 9, 10]. The vertical bars represent the 1σ statistical uncertainties. If the bars are not visible, they are smaller than the symbols. The solid line represents the recommendation from [11] used to calculate the production rate.

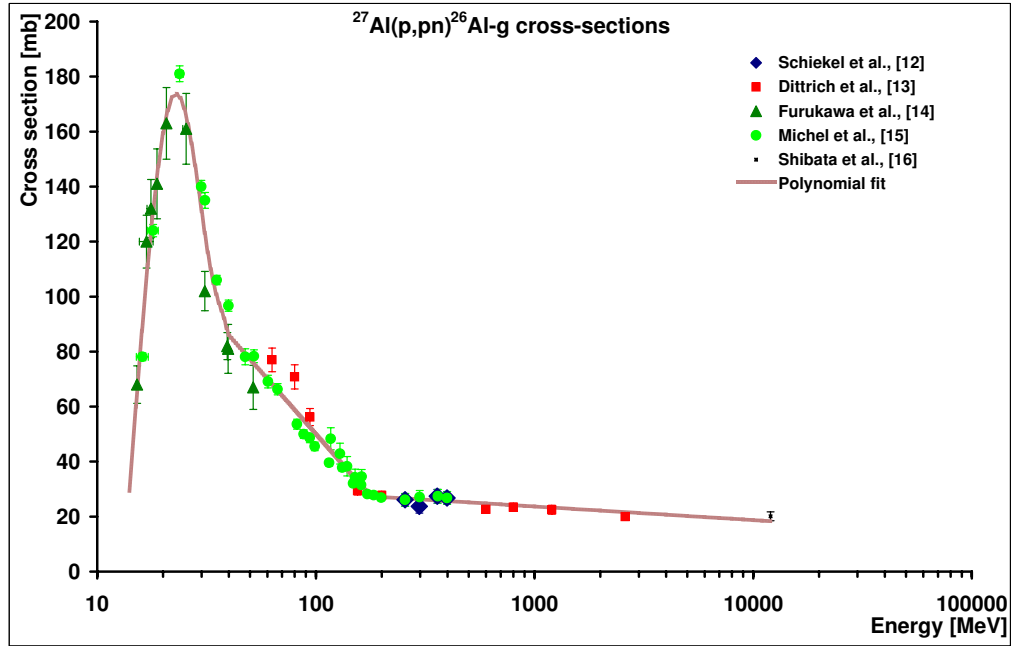


Figure 2: Measured production cross-sections for the reaction $^{27}\text{Al}(p,pn)^{26}\text{Al-g}$ [12, 13, 14, 15, 16]. The bars represent the 1σ statistical uncertainties. If the bars are not visible, they are smaller than the symbols. The solid line represents the polynomial fit to calculate the production rate.

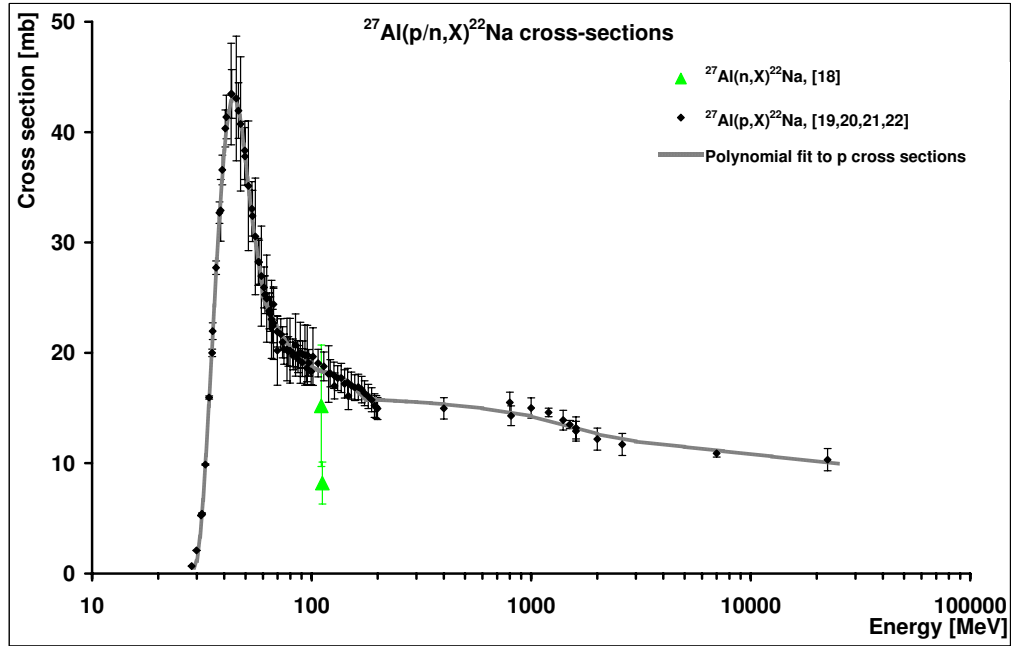


Figure 3: Measured production cross-sections for the reactions $^{27}\text{Al}(\text{n},2\text{p}4\text{n})^{22}\text{Na}$ (triangles) [18] and $^{27}\text{Al}(\text{p},3\text{p}3\text{n})^{22}\text{Na}$ (spades) [19, 20, 21, 22]. The bars represent the statistical 1σ uncertainties. If the bars are not visible, they are smaller than the symbols. The solid line represents the polynomial fit used to calculate the production rates.

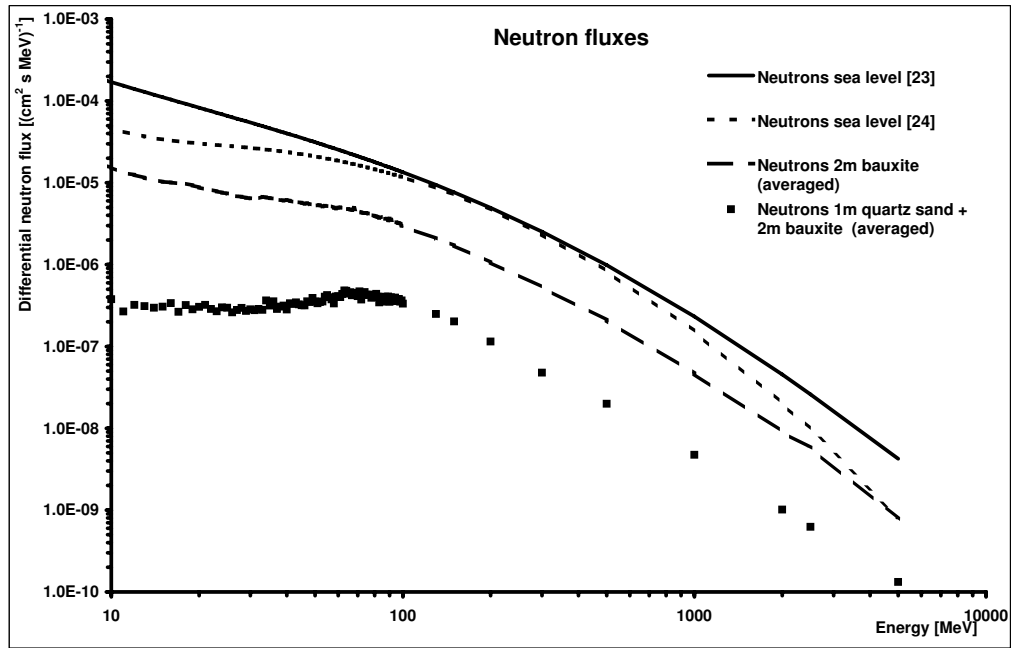


Figure 4: Differential parameterized neutron fluxes around New York, USA [23, 24] and the simulated neutron spectra averaged over a 2m thick bauxite layer with and without 1 m of quartz sand as top soil.

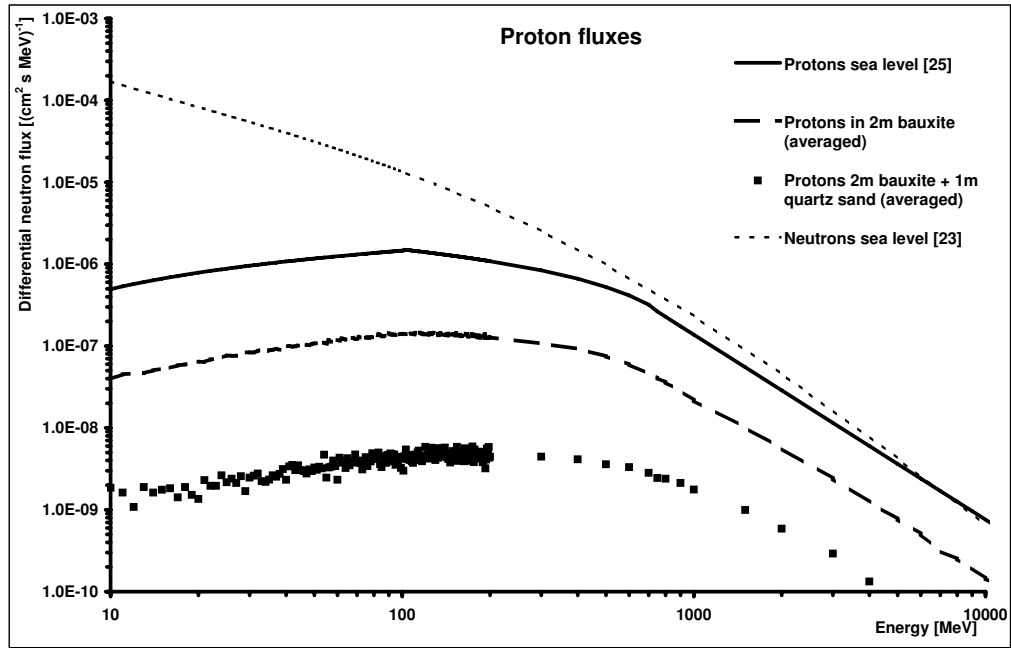


Figure 5: Differential parameterized proton flux [25] and the simulated proton spectra averaged over a 2 m thick bauxite layer with and without 1 m of quartz sand as top soil. The neutron flux at sea level [23] is given as reference.

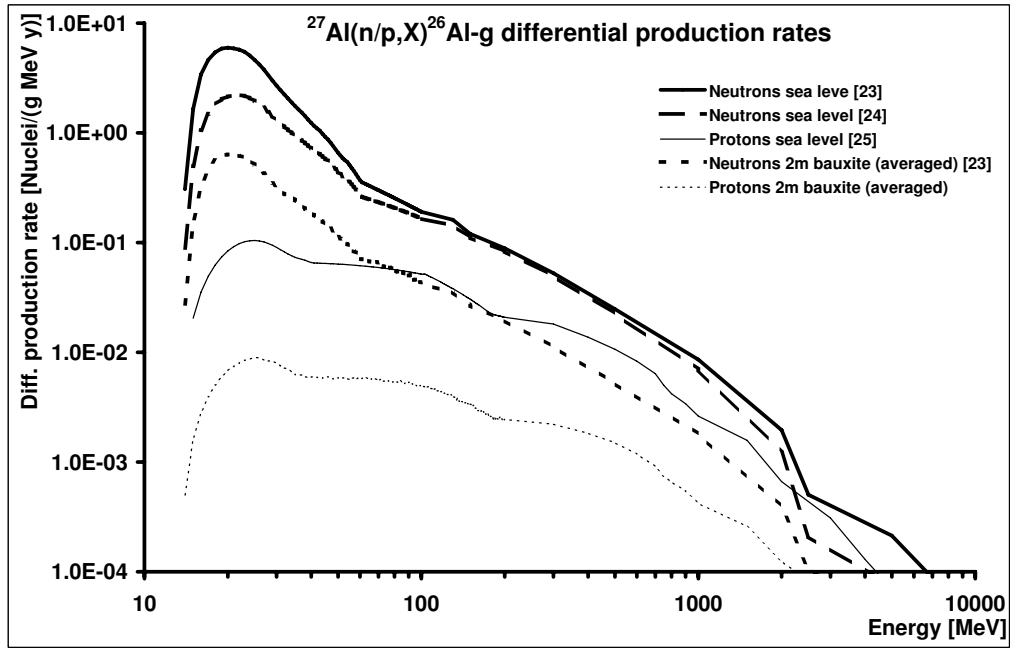


Figure 6: Calculated differential production rates of ^{26}Al in ^{27}Al due to secondary cosmic protons and neutrons at sea level and averaged over a 2 m thick bauxite layer without top soil.

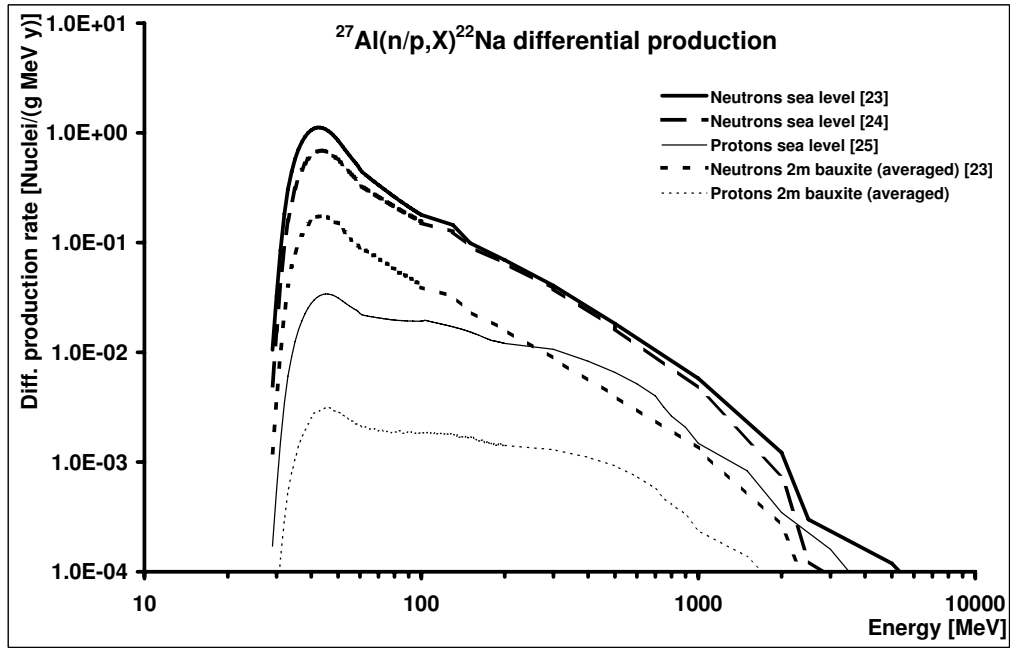


Figure 7: Calculated differential production rates of ^{22}Na in ^{27}Al due to secondary cosmic protons and neutrons at sea level and averaged over a 2 m thick bauxite layer without top soil.

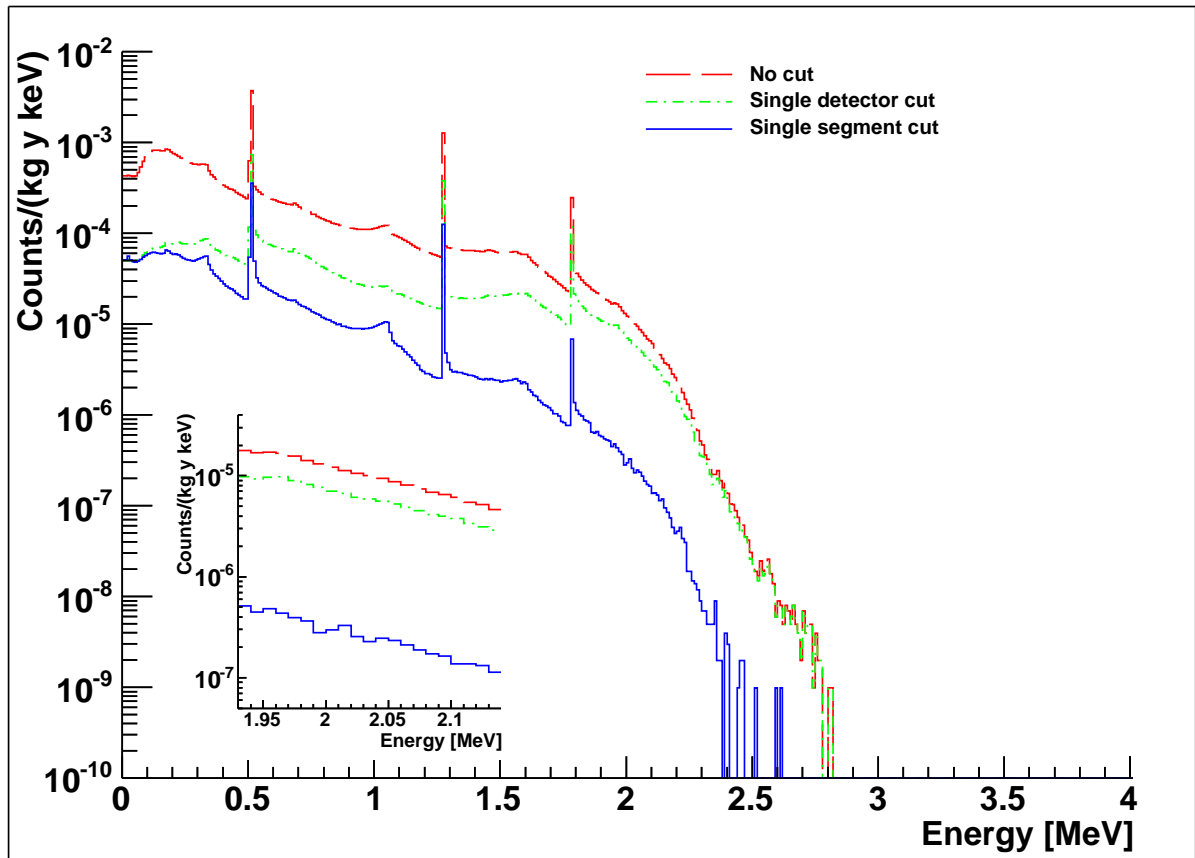


Figure 8: Simulated spectrum from a 1.0 mBq/kg ^{22}Na contamination in the metalization of HPGe detectors in a GERDA like setup [1]. Spectra are without any cut, with single detector cut and with single segment cut. The region of interest is shown in the inset.

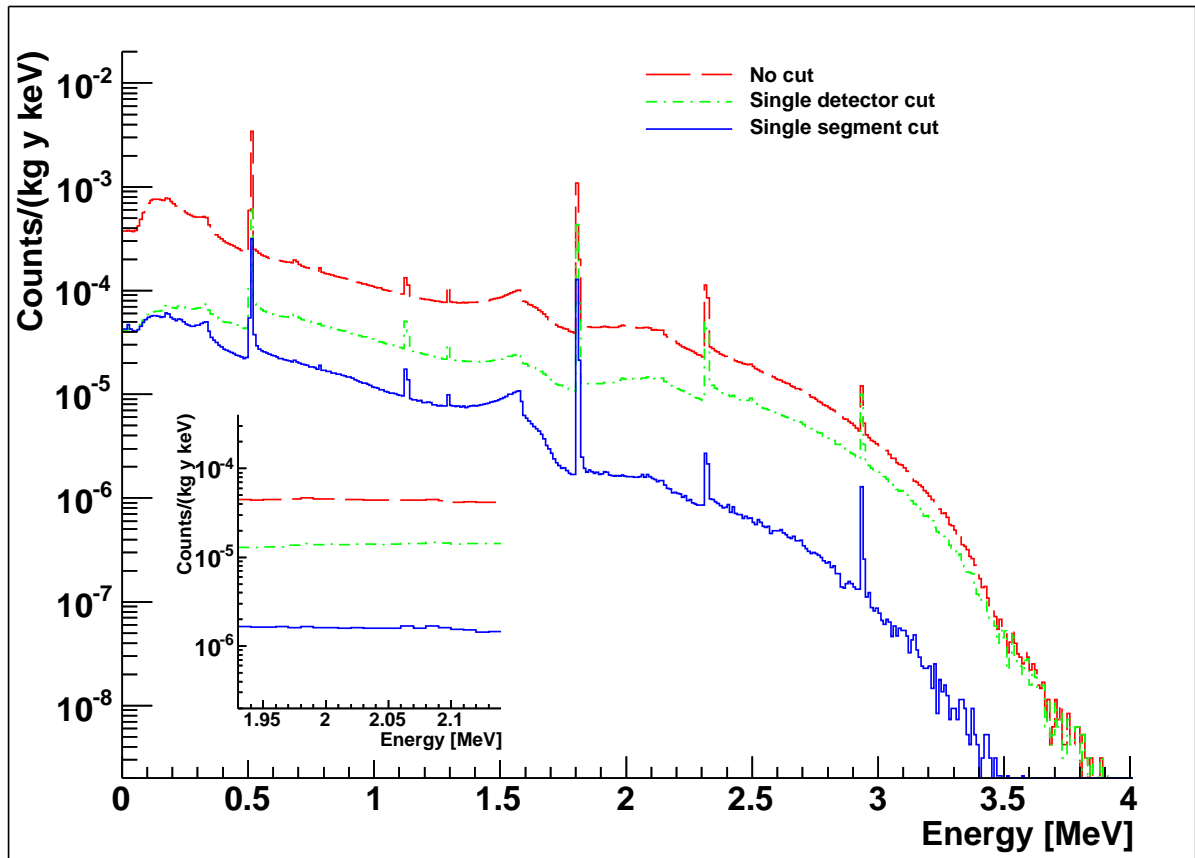


Figure 9: Simulated spectrum from a 1.0 mBq/kg ^{26}Al contamination in the metalization of HPGe detectors in a GERDA like setup [1]. Spectra are without any cut, with single detector cut and with single segment cut. The region of interest is shown in the inset.

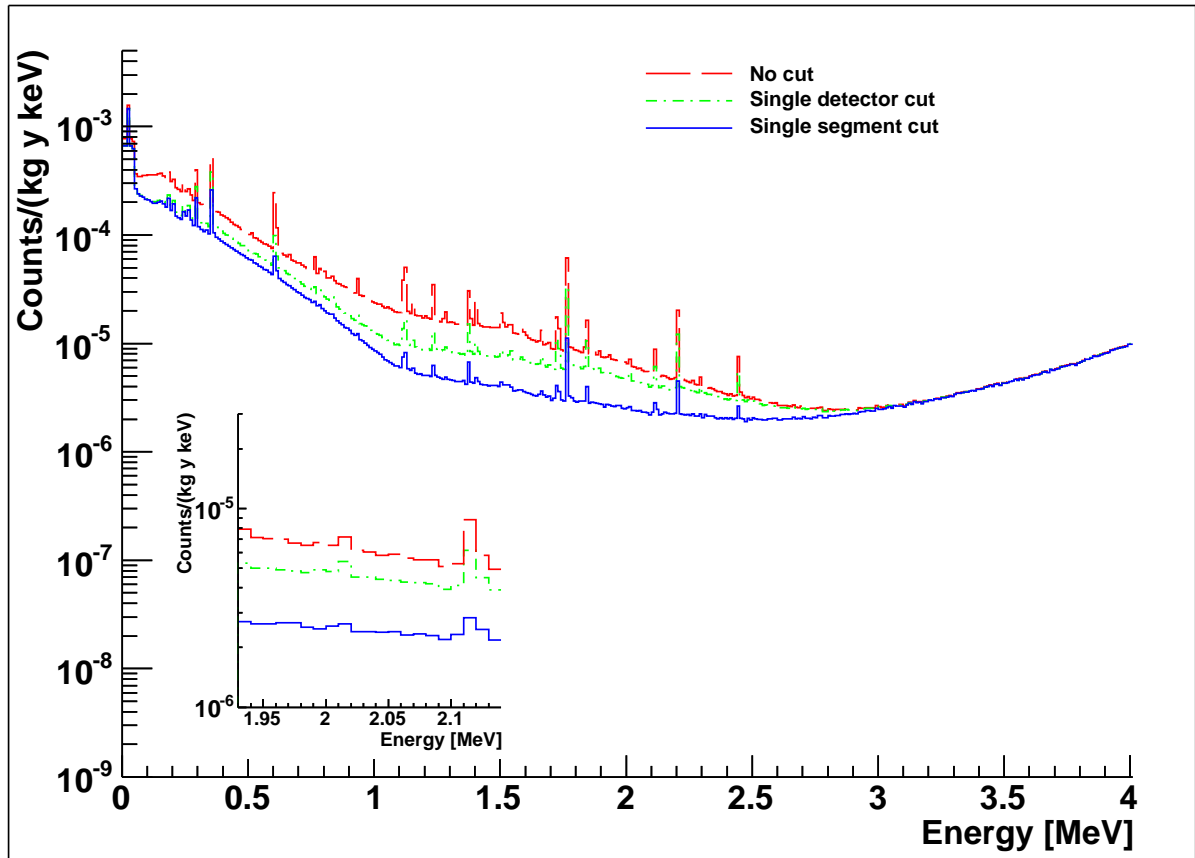


Figure 10: Simulated spectrum from a 1.0 mBq/kg ^{226}Ra contamination in the metalization of HPGe detectors in a GERDA like setup [1]. Spectra are without any cut, with single detector cut and with single segment cut. The region of interest is shown in the inset.

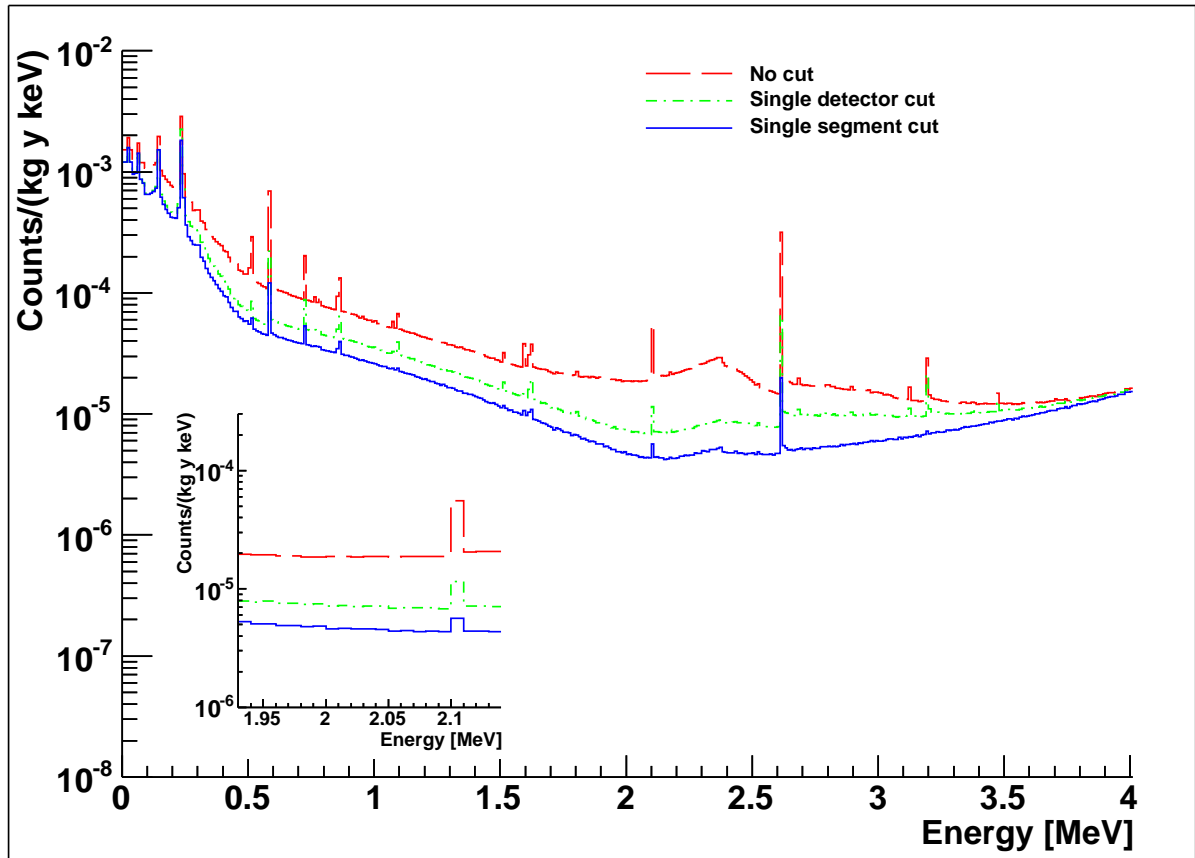


Figure 11: Simulated spectrum from a 1.0 mBq/kg ^{228}Th contamination in the metalization of HPGe detectors in a GERDA like setup [1]. Spectra are without any cut, with single detector cut and with single segment cut. The region of interest is shown in the inset.